British Journal of Pharmacology (2009), 156, 1326–1341

0007-1188/09
www.brjpharmacol.org

RESEARCH PAPER

Biochemical and behavioural characterization of EMPA, a novel high-affinity, selective antagonist for the OX_2 receptor

P Malherbe, E Borroni, L Gobbi, H Knust, M Nettekoven, E Pinard, O Roche, M Rogers-Evans, JG Wettstein and J-L Moreau

Discovery Research CNS, F. Hoffmann-La Roche Ltd., Basel, Switzerland

Background and purpose: The OX_2 receptor is a G-protein-coupled receptor that is abundantly found in the tuberomammillary nucleus, an important site for the regulation of the sleep-wake state. Herein, we describe the *in vitro* and *in vivo* properties of a selective OX_2 receptor antagonist, *N*-ethyl-2-[(6-methoxy-pyridin-3-yl)-(toluene-2-sulphonyl)-amino]-*N*-pyridin-3-ylmethyl-acetamide (EMPA).
Experimental approach: The affinity of [^{3}H]EMPA was assessed in membranes from HEK293-hOX_2-cells using saturation and binding kinetics. The antagonist properties of EMPA were determined by Schild analysis using the orexin-A- or orexin-B-induced accumulation of [^{3}H]inositol phosphates (IP). Quantitative autoradiography was used to determine the distribution and abundance of OX_2 receptors in rat brain. The *in vivo* activity of EMPA was assessed by reversal of [Ala^{11},D-Leu^{15}]orexin-B-induced hyperlocomotion during the resting phase in mice and the reduction of spontaneous locomotor activity (LMA) during the active phase in rats.
Key results: [^{3}H]EMPA bound to human and rat OX_2-HEK293 membranes with K_D values of 1.1 and 1.4 nmol·L^{-1} respectively. EMPA competitively antagonized orexin-A- and orexin-B-evoked accumulation of [^{3}H]IP at hOX_2 receptors with pA_2 values of 8.6 and 8.8 respectively. Autoradiography of rat brain confirmed the selectivity of [^{3}H]EMPA for OX_2 receptors. EMPA significantly reversed [Ala^{11},D-Leu^{15}]orexin-B-induced hyperlocomotion dose-dependently during the resting phase in mice. EMPA, injected i.p. in rats during the active phase, reduced LMA dose-dependently. EMPA did not impair performance of rats in the rotarod procedure.
Conclusions and implications: EMPA is a high-affinity, reversible and selective OX_2 receptor antagonist, active *in vivo*, which should prove useful for analysis of OX_2 receptor function.
British Journal of Pharmacology (2009) **156**, 1326–1341; doi:10.1111/j.1476-5381.2009.00127.x; published online 4 March 2009

Keywords: EMPA; orexin; OX_2 antagonist; binding kinetics; inositol phosphate accumulation; Schild analysis; autoradiography; rat brain distribution; orexin-B-induced hyperlocomotion; *ex vivo* receptor occupancy

Abbreviations: $[Ca^{2+}]_i$, intracellular calcium concentration; CHO, Chinese hamster ovary; CSF, cerebrospinal fluid; EMPA, *N*-ethyl-2-[(6-methoxy-pyridin-3-yl)-(toluene-2-sulphonyl)-amino]-*N*-pyridin-3-ylmethyl-acetamide; FLIPR, Fluorometric Imaging Plate Reader; GPCRs, G-protein-coupled receptors; IP, inositol phosphates; NREM, non-REM; REM, rapid eye movement; RT, reverse transcriptase

Introduction

The orexins/hypocretins, a family of hypothalamic neuropeptides, play an important role in modulating feeding behaviour, energy homeostasis and in regulating the sleep-wake cycle (Siegel, 2004; Ohno and Sakurai, 2008). The two members of the family, orexin-A/hypocretin-1 (33 amino acids) and orexin-B/hypocretin-2 (28 amino acids), are derived from the same precursor by proteolytic processing of the 130-amino-acid polypeptide prepro-orexin (de Lecea *et al.*, 1998; Sakurai *et al.*, 1998). Two receptor subtypes, termed OX_1 and OX_2, have been identified (nomenclature follows Alexander *et al.*, 2008). Characterization in binding and functional assays demonstrated that orexin-A is a non-selective neuropeptide that binds with similar affinities to OX_1 and OX_2 receptors, while orexin-B is selective and has a

Correspondence: Dr P Malherbe, F. Hoffmann-La Roche Ltd., Psychiatry Disease Area, Bldg. 69/333B, CH-4070 Basel, Switzerland. E-mail: parichehr.malherbe@roche.com
Received 1 September 2008; revised 6 November 2008; accepted 19 November 2008

10-fold higher affinity for OX_2 over OX_1 receptors (Sakurai *et al.*, 1998). Both receptors belong to the superfamily of G-protein-coupled receptors (GPCRs) that couple to $G_{q/11}$ and contribute to the activation of phospholipase C, leading to the elevation of intracellular Ca^{2+} concentrations, $[Ca^{2+}]_i$ (Sakurai *et al.*, 1998). In addition, a detailed signalling profile of human OX_2 receptors has recently shown that these receptors couple to G_s as well as $G_{q/11}$ and G_i pathways (Tang *et al.*, 2008). Northern blot analysis of adult rat tissues showed that prepro-orexin mRNA is detected exclusively in the brain, except for a small amount in the testis, and that OX_1 and OX_2 receptor transcripts are exclusively detected also in the brain (Sakurai *et al.*, 1998). The expression of orexins and their receptors have been detected by RT-PCR and immunohistochemistry in peripheral tissue including intestine, pancreas, adrenals, kidney and reproductive tract (Voisin *et al.*, 2003; Heinonen *et al.*, 2008). Distribution studies in rat brain using *in situ* hybridization and immunohistochemistry have shown that orexin neurons are found only in the lateral hypothalamic area yet having projections into the entire CNS (Peyron *et al.*, 1998; Nambu *et al.*, 1999). Although OX_1 and OX_2 receptors are present in most brain regions, OX_1 receptors are most abundantly expressed in the locus coeruleus while OX_2 receptors are expressed in regions controlling arousal, especially in the tuberomammillary nucleus, an important site for the regulation of sleep and wakefulness (Marcus *et al.*, 2001). The high expression of orexin receptors in brain regions such as neocortex L6, ventral tegmental area, locus coeruleus, preoptic area, dorsal and medial raphe nuclei and periaqueductal area, in combination with the projections of the hypothalamic orexin-containing neurons towards limbic and brain stem structures also are consistent with a crucial role for the orexin system in the complex regulation of emotional responses (Marcus *et al.*, 2001).

The disruption of orexin signalling is thought to be the cause of narcolepsy, an assumption based on several lines of evidence: prepro-orexin knockout (KO) mice presented a phenotype with characteristics remarkably similar to narcolepsy (Chemelli *et al.*, 1999); a mutation (*canarc-1*) that disrupts the gene encoding for OX_2 receptors was found to be responsible for canine narcolepsy (Lin *et al.*, 1999); a lack of orexin-A and orexin-B was observed in human narcoleptic patients (Nishino *et al.*, 2000; Peyron *et al.*, 2000); and it has been shown that modafinil, an anti-narcoleptic drug with unknown mechanism of action, activates orexin neurons (Chemelli *et al.*, 1999). Intracerebroventricular (i.c.v.) administration of orexin-A was shown to dose-dependently increase the wake time and reduce total rapid eye movement (REM) sleep by 84% in rats (Piper *et al.*, 2000). Wakefulness induced by orexin-A is likely to be mediated by the histaminergic system through OX_2 receptors and is almost completely absent in H_1 receptor KO mice (Huang *et al.*, 2001; Yamanaka *et al.*, 2002). Interestingly, a non-selective H_1 antagonist pyrilamine attenuated the effect of i.c.v. injected orexin-A on wakefulness in rats (Yamanaka *et al.*, 2002). OX_2 receptor KO mice exhibit abnormal attacks of non-REM (NREM) sleep and marked sleep-wake fragmentation along with mild cataplexy (Willie *et al.*, 2003). Taken together, these observations are consistent with a vital role for the orexin system, and especially OX_2 receptors, in the modulation of sleep. Indeed, recent preclinical (dog and rat) and phase I (healthy male subjects; single dose) investigations have shown that the dual OX_1/OX_2 receptors antagonist almorexant (ACT-078573) promoted sleep (NREM and REM) in animals and humans without disrupting sleep architecture, an action that validated the notion that OX receptor antagonists could be effective hypnotics for the treatment of insomnia (Brisbare-Roch *et al.*, 2007). Moreover, the orexin neuronal system has also been implicated in pain modulation within the CNS (Holland and Goadsby, 2007). The genetic linkage and haplotype analyses have shown an association between the OX_2 receptor gene and cluster headaches (Rainero *et al.*, 2007; 2008). The G1246A polymorphism (substitution of valine 308 by isoleucine) of the OX_2 gene has been suggested to modulate the genetic risk for cluster headaches by interfering with the dimerization process of OX_2 receptors (Rainero *et al.*, 2008).

Given the diverse functioning of orexin systems, selective antagonists targeted at OX_1 or OX_2 receptors can provide crucial tools for deciphering and understanding the physiological and pathophysiological roles of each receptor subtype. SB-334867-A, (1-(2-methylbenzoxazol-6-yl)-3-[1,5] naphthyridin-4-yl-urea hydrochloride) was the first non-peptide OX_1 receptor antagonist reported (Smart *et al.*, 2001). SB-334867-A has been intensively used for *in vivo* studies of orexin-A physiological effects (Nishino, 2007). *N*-(4-pyridylmethyl)(*S*)-*tert*-leucyl-6,7-dimethoxy-1,2,3,4-tetrahydroisoquinoline was the first non-peptide selective OX_2 receptor antagonist to be described (Hirose *et al.*, 2003). Until now, there was a lack of selective radioligands for OX_2 receptors. In the current study, the binding characteristics of the selective OX_2 receptor antagonist radioligand, [^{3}H]*N*-ethyl-2-[(6-methoxy-pyridin-3-yl)-(toluene-2-sulphonyl)-amino]-*N*-pyridin-3-ylmethyl-acetamide ([^{3}H]EMPA), to cell membranes from HEK293 cells expressing hOX_2 receptors and to rat brain sections are described. Data show that EMPA is a potent, highly selective and reversible antagonist of OX_2 receptors and that it displays *in vivo* activity in the reversal of [Ala^{11},D-Leu^{15}]orexin-B-induced hyperlocomotion in mice and a decrease of spontaneous locomotion during the active phase in rats.

Methods

Plasmids, cell culture and membrane preparation

cDNA encoding human OX_2 (Accession No. O43614), rat OX_2 (Accession No. P56719) and human OX_1 receptors (Accession No. O43613) were subcloned into pCI-Neo expression vectors (Promega, Madison, WI). HEK293 cells were transfected as previously described (Malherbe *et al.*, 2006). After 48 h post-transfection, cells were harvested and washed 3 times with cold PBS and frozen at –80°C. The pellet was suspended in ice-cold buffer containing 15 mmol·L^{-1} Tris-HCl, pH 7.5, 2 mmol·L^{-1} $MgCl_2$, 0.3 mmol·L^{-1} EDTA, 1 mmol·L^{-1} EGTA, protease inhibitor cocktail EDTA-free (Cat. No. 11 873 580 001, Roche Applied Science, RAS, Rotkreuz, Switzerland) and homogenized with a Polytron (Kinematica AG, Basel, Switzerland) for 30 s at 16 000 r.p.m. After centrifugation at 48 000× *g* for 30 min at 4°C, the pellet was suspended in ice-cold buffer containing

75 mmol·L^{-1} Tris-HCl, pH 7.5, 12.5 mmol·L^{-1} $MgCl_2$, 0.3 mmol·L^{-1} EDTA, 1 mmol·L^{-1} EGTA, 250 mmol·L^{-1} sucrose, protease inhibitor cocktail EDTA-free. After homogenization for 15 s at 16 000 r.p.m., protein content was measured using the BCA method (Pierce, Socochim, Lausanne, Switzerland) with bovine serum albumin as the standard. The membrane homogenate was frozen at –80°C before use.

[^{3}H]EMPA binding

After thawing, membrane homogenates were centrifuged at 48 000× *g* for 10 min at 4°C, pellets were re-suspended in the binding buffer (25 mmol·L^{-1} HEPES, pH 7.4, 1 mmol·L^{-1} $CaCl_2$, 5 mmol·L^{-1} $MgCl_2$, 0.5% BSA, 0.05% Tween 20) to a final assay concentration of 2.5 µg protein per well. Saturation isotherms were determined by the addition of various concentrations of [^{3}H]EMPA to these membranes (in a total reaction volume of 500 µL) for 60 min at 23°C. At the end of incubation, membranes were filtered onto unitfilter, a 96-well white microplate with bonded GF/C filter pre-incubated 1 h in wash buffer (25 mmol·L^{-1} HEPES, pH 7.4, 1 mmol·L^{-1} $CaCl_2$, 5 mmol·L^{-1} $MgCl_2$) plus 0.5% polyethylenimine, with a Filtermate 196 harvester (PerkinElmer Life and Analytical Sciences, Waltham, MA) and washed 4 times with ice-cold wash buffer. Non-specific binding (NSB) was measured in the presence of 10 µmol·L^{-1} EMPA. Radioactivity on the filter was counted (5 min) on a Top-Count microplate scintillation counter (PerkinElmer Life and Analytical Sciences) with quenching correction after addition of 45 µL of microscint 40 (PerkinElmer Life and Analytical Sciences) and shaking for 1 h.

Saturation experiments were analysed by Prism 4.0 (GraphPad software, San Diego, CA) using the rectangular hyperbolic equation derived from the equation of a bimolecular reaction and the law of mass action, $B = (B_{max} * [F])/(K_D + [F])$, where B is the amount of ligand bound at equilibrium, B_{max} is the maximum number of binding sites, [F] is the concentration of free ligand and K_D is the ligand dissociation constant. For inhibition experiments, membranes were incubated with [^{3}H]EMPA at a concentration equal to the K_D value of radioligand and 10 concentrations of the inhibitory compound (0.0001–10 µmol·L^{-1}). IC_{50} values were derived from the inhibition curve and the affinity constant (K_i) values were calculated using the Cheng-Prussoff equation $K_i = IC_{50}/(1 + [L]/K_D)$ where [L] is the concentration of radioligand and K_D is its dissociation constant at the receptor, derived from the saturation isotherm. To measure association kinetics, membranes were incubated at 23°C in the presence of radioligand (~1.1 nmol·L^{-1} [^{3}H]EMPA) for 0, 1, 3, 5, 7, 10, 15, 20, 30, 60, 90 or 120 min, then terminated by rapid filtration. Dissociation kinetics were measured by adding at different times before filtration, 10 µmol·L^{-1} EMPA to membranes pre-incubated at 23°C for 1 h in the presence of ~1.1 nmol·L^{-1} [^{3}H]EMPA. Binding kinetics parameters, K_{ob} and K_{off} values (observed on and off rates), were derived from association-dissociation curves using the one phase exponential association and decay equations (Prism 4.0, GraphPad software) respectively. K_{on}, half-life and K_d were calculated using the $K_{on} = (K_{ob} - K_{off})/[ligand]$, $t_{1/2} = \ln 2/K$ and $K_D = K_{off}/K_{on}$ equations respectively.

Accumulation of [^{3}H]inositol phosphates (IP)

Accumulation of [^{3}H]IP was measured as described previously (Malherbe *et al.*, 2006) with the following adaptations. The Chinese hamster ovary (CHO) (dHFr$^-$) mutant cell line stably expressing human OX_2 receptors, CHO(dHFr$^-$)-hOX_2, was maintained in Dulbecco's modified Eagle's medium (DMEM; 1×) with GlutaMax™1, 4500 mg·L^{-1} D-glucose and sodium pyruvate, 5% dialysed fetal calf serum, 100 µg·mL^{-1} penicillin and 100 µg·mL^{-1} streptomycin (Pen/Strep). Cells were washed twice in labelling medium: DMEM without inositol (MP Biomedicals, Irvine, CA), 10% dialysed FCS, 1% Pen/Strep, 2 mmol·L^{-1} glutamate. Cells were seeded at 8×10^4 cells per well in poly-D-lysine-treated 96-well plates in the labelling medium supplemented with 5 µCi·mL^{-1} of myo-[1,2-^{3}H]-inositol and were incubated overnight. The following day, cells were washed 3 times with the wash buffer (1 × HBSS, 20 mmol·L^{-1} HEPES, pH 7.4) and then incubated for 10 min at 23°C in assay buffer (1 × HBSS, 20 mmol·L^{-1} HEPES, pH 7.4, 0.1% BSA, plus 8 mmol·L^{-1} LiCl to prevent phosphatidylinositide breakdown), prior to the addition of agonists or antagonists. When present, antagonists were incubated for 20 min at 23°C prior to stimulation with agonist; concentrations ranged from 0.00003 to 3 µmol·L^{-1} for orexin-A and 0.0001 to 10 µmol·L^{-1} for orexin-B. After 45 min incubation at 37°C with agonist, the assay was terminated by the aspiration of the assay buffer and the addition of 100 µL 20 mmol·L^{-1} formic acid to the cells. After shaking for 30 min at 23°C, a 40 µL aliquot was mixed with 80 µL of yttrium silicate beads (12.5 mg·mL^{-1}) that bind to the IP (but not inositol) and shaken for 30 min at 23°C. Assay plates were centrifuged for 2 min at 750× *g* prior to counting on a Packard Top-count microplate scintillation counter with quenching correction (PerkinElmer Life and Analytical Sciences).

Intracellular Ca^{2+} mobilization assay

The CHO(dHFr$^-$)-hOX_1 and -hOX_2 stable cells lines were seeded at 5×10^4 cells per well in the poly-D-lysine treated, 96-well, black/clear-bottomed plates. Twenty-four hous later, cells were loaded for 1 h at 37°C with 4 µmol·L^{-1} Flou-4 acetoxymethyl ester in FLIPR buffer (1 × HBSS, 20 mmol·L^{-1} HEPES, 2.5 mmol·L^{-1} Probenecid). Cells were washed 5 times with FLIPR buffer to remove excess dye and intracellular calcium mobilization; $[Ca^{2+}]_i$ were measured using a Fluorometric Imaging Plate Reader (FLIPR-96, Molecular Devices, Menlo Park, CA) as described previously (Malherbe *et al.*, 2006). Orexin-A or orexin-B (50 mmol·L^{-1} stock solution in DMSO) were diluted in FLIPR buffer plus 0.1% BSA. The EC_{50} and EC_{80} values of orexin were measured daily from standard agonist concentration-response curves in CHO(dHFr$^-$)-hOX_1 or -OX_2 receptor stable cell line. All compounds were dissolved in 100% DMSO, and diluted in FLIPR buffer to a 5× stock (2.5% DMSO). This stock was then applied to the cells at a final DMSO concentration of 0.5%. Inhibition curves were determined by addition of 11 concentrations (0.0001–10 µmol·L^{-1} in FILPR buffer) of inhibitory compounds and using EC_{80} value of orexin-A or orexin-B as agonist (a concentration which gave 80% of maximum agonist response, determined daily). The antagonists were applied 25 min (incubation at 37°C) before the application of the agonist.

Responses were measured as peak increase in fluorescence minus basal, normalized to the maximal stimulatory effect induced by EC_{80} value of orexin-A or orexin-B. Inhibition curves were fitted according to the Hill equation: $y = 100/(1+(x/IC_{50})^{nH})$, where n_H = slope factor using Prism 4.0 (GraphPad software). K_b values were calculated according to the following equation $K_b = IC_{50}/(1 + [A]/EC_{50})$, where A is the concentration of agonist added that is very close to agonist EC_{80} value, and IC_{50} and EC_{50} values were derived from the antagonist inhibition and orexin agonist curves respectively.

Radioligand binding to tissue sections and quantitative receptor autoradiography

All animal care and experimental procedures were approved by the City of Basel Cantonal Animal Protection Committee, based on adherence to Federal and local regulations. Mice and rats were housed in separate holding rooms at controlled temperature (20–22°C) and 12 h light/dark cycle (lights on 06:00 h). All animals were allowed *ad libitum* access to food and water.

Male CD Sprague-Dawley rats weighing 150–180 g were killed by decapitation; brains were rapidly dissected and immediately frozen in dry ice. Coronal cryostat-cut sections (10 µm thick) were mounted on Histobond glass slides (Marienfeld Laboratories Glassware, Germany) dried at room temperature and stored at –20°C. Sections were pre-incubated 2 × 10 min in assay buffer (1 mmol·L^{-1} $CaCl_2$, 5 mmol·L^{-1} $MgCl_2$, 25 mmol·L^{-1} HEPES, pH 7.4) and then for 60 min in assay buffer containing 1 nmol·L^{-1} [^{3}H]EMPA (all incubations at room temperature). Sections were then rinsed in 2 × 5 min in ice-cold assay buffer (2 × 5 min). This was followed by three rapid washes in distilled water at 4°C. NSB was determined in the presence of 10 µmol·L^{-1} Cp-5 or other orexin receptor antagonists.

Brain sections were exposed, together with tritium microscales, to tritium-sensitive imaging plates (BAS-TR2025) for 5 days. Plates were scanned in a Fujifilm BAS-5000 high resolution phosphor imager and images quantified with an MCID M2 image analysis system (Imaging Research Inc., St. Catherines, Ontario, Canada). Sections were then stained with cresyl violet, photographed and pictures obtained were compared with a parent autoradiogram to allow unambiguous identification of the regions displaying binding of [^{3}H]EMPA.

Determination of OX_2 receptor occupancy using ex vivo [^{3}H]EMPA autoradiography

Male CD Sprague-Dawley rats were given vehicle (1% Tween-80 in physiological saline) or almorexant (3, 10 or 30 mg·kg^{-1}) (i.p., $n = 2$ per group). Thirty minutes after dosing, animals were sacrificed by decapitation; brains were rapidly dissected and immediately frozen in dry ice. Cryostat coronal sections were processed for [^{3}H]EMPA receptor autoradiography as described above.

Pharmacokinetics of EMPA in mice and rats

Pharmacokinetic experiments were performed in male NMRI mice and Wistar rats. Mice were dosed either i.v. (into the tail vain) or p.o. (microsuspension, as a gavage). At defined time points, terminal plasma and brain tissue was collected. Two mice per group were killed at 0.083, 0.333, 1, 2, 4 and 7 h after the i.v. administration of 10.77 mg·kg^{-1} EMPA or 0.25, 0.5, 1, 2, 4 and 7 h after the p.o. administration of 18.04 mg·kg^{-1} EMPA. Rats were given a single oral dose (19.71 mg·kg^{-1}, microsuspension, as a gavage) or i.v. (11.79 mg·kg^{-1}, via a jugular vein). Plasma and brain samples were collected after killing from two rats per group at 0.083, 0.25, 0.5, 1, 2, 4 and 8 h (i.v.) or 0.25, 0.5, 1 and 2 h (p.o.) after dosing. Concentrations of EMPA were determined using quantitative liquid chromatography/mass spectrometry/mass spectrometry (LC/MS/MS). Pharmacokinetic parameters were calculated by non-compartmental analysis of plasma concentration-time curves using WinNonlin, version 4.1 software (Pharsight Corporation, Mountain View, CA).

In vivo evaluation of EMPA

Animals and drug treatment

Male NMRI mice (20–30 g) supplied from Iffa Credo, Lyon, France and Male Wistar rats (196–237 g) supplied from RCC Ltd., Fullinsdorf, Switzerland were used. EMPA was prepared immediately prior to use in 0.3% (w/v) Tween-80 in physiological saline (0.9% NaCl) and injected i.p. at a volume of 10 mL·kg^{-1} body weight for mice and 5 mL·kg^{-1} for rats. All doses are expressed as that of the base.

Reversal of [Ala^{11},D-Leu^{15}]orexin-B-induced hyperlocomotion in mice

A computerized Digiscan 16-Animal Activity Monitoring System (Omnitech Electronics, Colombus, OH) was used to quantify locomotor activity (LMA). Data were obtained simultaneously from eight Digiscan activity chambers placed in a soundproof room with a 12 h light/dark cycle. All tests were performed during the light phase (6 AM to 6 PM). Each activity monitor consisted of a Plexiglas box (20 × 20 × 30.5 cm) with sawdust bedding on the floor surrounded by invisible horizontal and vertical infrared sensor beams. Cages were connected to a Digiscan Analyzer linked to a PC that constantly collected the beam status information. The activity detector operates by counting the number of times the beams change from uninterrupted to interrupted or *vice versa*. Records of photocell beam interruptions, for individual animals, typically were taken every 5 min over the duration of the test session. Mice were first transferred from home cages to recording chambers for a 50 min habituation phase during which they were allowed to freely explore the new environment. Mice were then injected i.p. with EMPA (1, 3, 10, 30, 100, 300 mg·kg^{-1}, $n = 8$ mice per dose). Ten minutes later, mice were briefly anaesthetized with isoflurane inhalation to allow i.c.v. injection of 5 µL of either artificial cerebrospinal fluid (CSF) or [Ala^{11},D-Leu^{15}]orexin-B at a dose of 3 µg. Mice were then immediately replaced in the test compartments and LMA was recorded during the following 30 min.

Spontaneous locomotor activity in rats during the dark (active) phase

Male Wistar rats (~150 g at arrival) housed four per cage (Makrolon cages 1800 cm^2) with free access to food and water were allowed 2 weeks of acclimatization to a reversed light/dark animal room (dark cycle: 10.00 AM to 10.00 PM) prior to testing. On test days, LMA was monitored by a computerized Digiscan Animal Activity Monitoring system as described above (Omnitech Electronics, Columbus, OH). The activity monitoring chambers were made of Plexiglas (41 × 41 × 30 cm W × L × H) and contained a thin layer of sawdust bedding. One rat per cage was monitored at the same time. One hour after the dark period onset, rats were injected i.p. with EMPA (3, 10, 30 $mg \cdot kg^{-1}$, $n = 8$ rats per dose) and immediately placed into the activity monitoring chambers. LMA was then recorded in 5 min time bins for a period of 30 min.

Motor coordination and balance in rats

Male Wistar rats (~200 g body weight) were trained to remain on a horizontal metal rod (rotarod, Ugo Basile, Biological Research Apparatus, Varese, Italy) rotating at a fixed speed until criterion level (120 s on rod) was reached. The rotarod was 7 cm wide, 5 cm in diameter and 25 cm above the bench. The following day, animals were injected i.p. with vehicle or EMPA (3, 10 or 30 $mg \cdot kg^{-1}$; $n = 8$ per group). Animals were tested for rotarod performance at 8 r.p.m. and then at 16 r.p.m. (total time spent on the rod, maximum 120 s) 10 min after injection. Rats were allowed a maximum of three trials to remain on the rotarod for 120 s; assessment terminated when the animal fell from the rotarod or reached criterion level. The mean time over the number of trials completed per rat was calculated.

Statistics

All parameters were analysed with a repeated measure ANOVA, followed in significant cases by a Dunnett's *t*-test. A *P*-value of 0.05 was accepted as statistically significant.

Materials

EMPA (*N*-ethyl-2-[(6-methoxy-pyridin-3-yl)-(toluene-2-sulphonyl)-amino]-*N*-pyridin-3-ylmethyl-acetamide, WO2004033418A2), almorexant (ACT-078573, (*R*)-2-{(*S*)-6,7-dimethoxy-1-[2-(4-trifluoromethyl-phenyl)-ethyl]-3,4-dihydro-1H-isoquinolin-2-yl}-*N*-methyl-2-phenyl-acetamide, WO2005118548-A1) (Brisbare-Roch *et al.*, 2007), Cp-1 ((*R*)-2-{(*S*)-6,7-dimethoxy-1-[2-(6-trifluoromethyl-pyridin-3-yl)-ethyl]-3,4-dihydro-1H-isoquinolin-2-yl}-*N*-methyl-2-phenyl-acetamide, WO2005118548-A1), Cp-2 (1-(9-oxo-8-trifluoromethyl-1,2,3,9-tetrahydro-pyrrolo[2,1-*b*]quinazolin-3-yl)-1-((*S*)-1-phenyl-ethyl)-3-(2-trifluoromethoxy-phenyl)-urea, WO2004004733 A1), Cp-3 (2-methyl-5-phenyl-thiazole-4-carboxylic acid cyclobutyl-[3-(4-fluoro-phenoxy)-propyl]-amide, WO2006110626A1), Cp-4 (2-[[4-chloro-2-(hydroxy-phenyl-methyl)-phenyl]-(3,4-dimethoxybenzenesulphonyl)-amino]-*N*-methyl-acetamide, WO2006024779-A1), Cp-5 ((*S*)-1-(6,7-dimethoxy-3,4-dihydro-1H-isoquinolin-2-yl)-3,3-dimethyl-2-[(pyridin-4-ylmethyl)-amino]-butan-1-one, WO2001085693-A1) (Hirose *et al.*, 2003), and SB 674042 (1-(5-(2-fluoro-phenyl)-2-methyl-thiazol-4-yl)-1-((S)-2-(5-phenyl-(1,3,4)oxadiazol-2-ylmethyl)-pyrrolidin-1-yl)-methanone) (Langmead *et al.*, 2004) were synthesized in the chemistry department of F. Hoffmann-La Roche according to procedures described in patent literature. [^{3}H]EMPA (specific activity: 94.3 Ci $mmol^{-1}$) and [^{3}H]SB 674042 (specific activity: 24.4 Ci $mmol^{-1}$) were synthesized by Drs Philipp Huguenin and Thomas Hartung at the Roche chemical and isotope laboratories, Basel, Switzerland. SB 334867 (N-(2-methyl-6-benzoxazolyl)-N''-1,5-naphthyridin-4-yl urea) (Tocris 1960), orexin-A (Tocris 1455), orexin-B (Tocris 1456) and [Ala^{11},D-Leu^{15}]orexin-B (Tocris 2142) were purchased from Tocris Bioscience (Bristol, UK). [*myo*-1,2-^{3}H]inositol with PT6-271 (TRK911, specific activity: 16.0 Ci $mmol^{-1}$; GE Healthcare, Chalfont St. Giles, UK) and yttrium silicate RNA binding beads (RPNQ0013) were purchased from GE Healthcare.

Results

Characterization of [^{3}H]EMPA binding and displacement studies

EMPA was previously described in the patent WO2004033418A2 to be a selective OX_2 receptor antagonist. For the current study, EMPA was tritiated ([^{3}H]EMPA, Figure 1). To characterize the *in vitro* binding of [^{3}H]EMPA, saturation binding analysis was performed at binding equilibrium (1 h incubation at 23°C), on membranes isolated from the HEK293 transiently transfected with the human and rat OX_2 receptors. The saturation isotherm and Scatchard plot of [^{3}H]EMPA binding to human OX_2-HEK293 cell membranes are shown in Figure 2A. The saturation isotherm was monophasic ([^{3}H]EMPA concentrations 0.01–12 $nmol \cdot L^{-1}$) and best fitted to a one-site model. Similarly, the Scatchard plot was linear (see inset of Figure 2A).

Binding kinetics of [^{3}H]EMPA to membrane preparations from HEK293 cells transiently expressing hOX_2 receptors are shown in Figure 2B and C and the kinetic parameters in Table 1. The association binding of [^{3}H]EMPA to the hOX_2 receptors was rapid with half-maximal binding occurring at 6.3 min and reaching equilibrium within 20 min. The data were fitted by a one-phase exponential model with the association rate constant of 0.028 ± 0.06 $nmol \cdot L^{-1} \cdot min^{-1}$. The dissociation rate for [^{3}H]EMPA binding to the hOX_2 receptors was determined by the addition of an excess amount of EMPA after equilibrium was reached. The reversal of binding for EMPA was complete with $t_{1/2}$ value of 9 min. The calculations of the apparent K_D value derived from the kinetic experiments was 2.74 ± 0.20, which was higher than that of equilibrium K_D value of 1.1 ± 0.1 $nmol \cdot L^{-1}$.

[^{3}H]SB 674042, an OX_1 receptor selective radioligand antagonist, binding to hOX_1 membrane was previously described (Langmead *et al.*, 2004). Hence, the selectivity of EMPA for OX_2 versus OX_1 receptors was determined using [^{3}H]SB 674042 and [^{3}H]EMPA competition binding assays to the membranes isolated from the HEK293 transiently transfected with the hOX_1 and hOX_2 receptors. As seen in Figure 3A, [^{3}H]SB 674042 was weakly displaced by EMPA from hOX_1 membrane with IC_{50} = 1900.0 ± 157.0 $nmol \cdot L^{-1}$, K_i = 900.0 ± 67.0 $nmol \cdot L^{-1}$, n_H = 1.0 ± 0.0. While [^{3}H]EMPA was strongly displaced by EMPA from hOX_2 membrane with

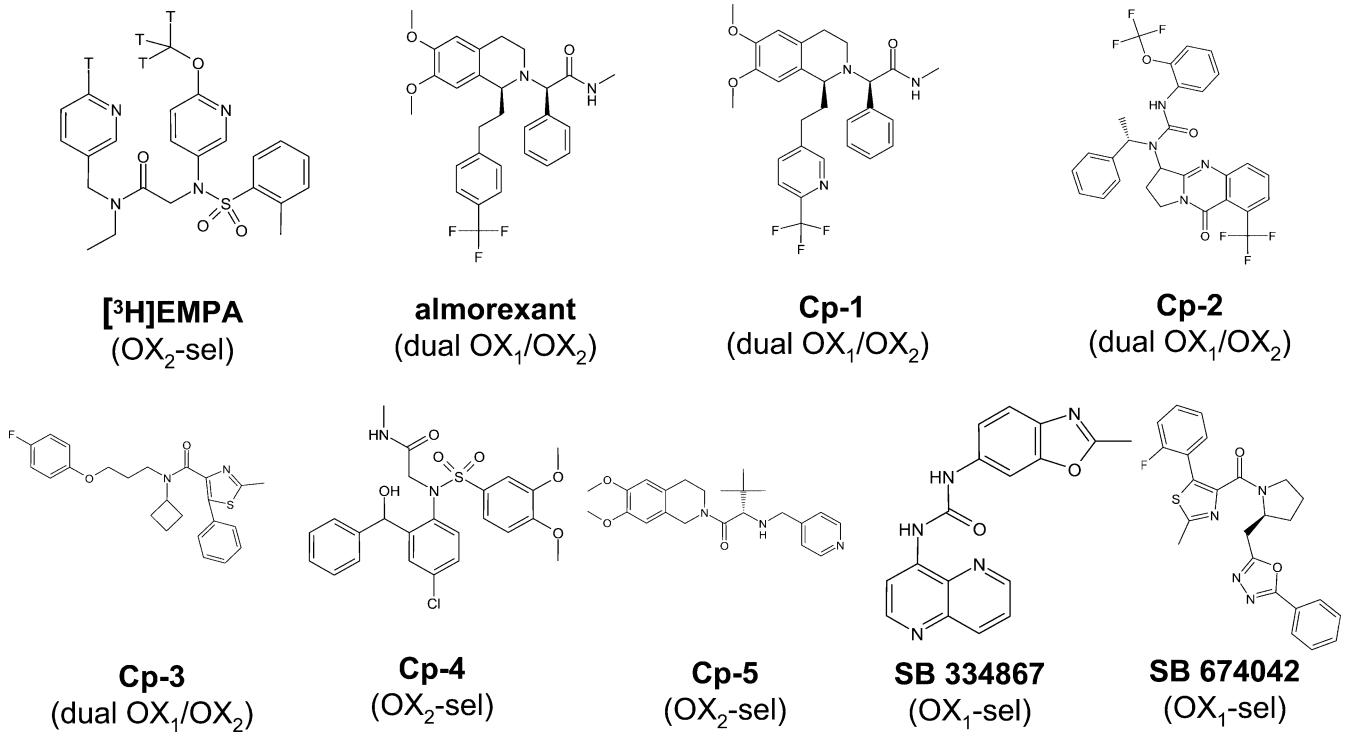

Figure 1 Chemical structures of the selective OX_1, OX_2 and dual OX_1/OX_2 receptor antagonists. T, tritium.

IC_{50} = 2.3 ± 0.5 nmol·L^{-1}, K_i = 1.1 ± 0.2 nmol·L^{-1}, n_H = 1.0 ± 0.0. Furthermore, to assess the pharmacological profile of [^{3}H]EMPA in competition binding assay, selective OX_1, OX_2 and dual OX_1/OX_2 receptor antagonists that had been previously described in the patent literature were synthesized: the selective OX_1 receptor antagonists SB 334867 (Smart *et al*., 2001) and SB 674042 (Langmead *et al*., 2004); selective OX_2 receptor antagonists Cp-4 and Cp-5 (Hirose *et al*., 2003) and dual OX_1/OX_2 receptor antagonists almorexant (Brisbare-Roch *et al*., 2007), Cp-1, Cp-2 and Cp-3 are shown in Figure 1. Potencies of these antagonists in inhibition of [^{3}H]EMPA binding to hOX_2-HEK293 cell membranes are shown in Figure 3B with K_i and n_H values in Table 2.

Of note is the use of two cell systems for binding (HEK293 cells transiently transfected with hOX_2 receptors) and functional studies [FLIPR and IP accumulation assays using CHO(dHFr$^-$)-hOX_2 receptor stable cell in the current study]. As HEK293 cells were adapted to grow and be transiently transfected in suspension in spinner flasks, it was possible to produce and prepare large quantities of transfected cells and membranes required for binding studies. Experiments with membranes prepared from HEK293-hOX_2 and CHO(dHFr$^-$)-hOX_2 cell systems showed similar K_D values (1.1 vs. 0.7 nmol·L^{-1}) for [^{3}H]EMPA binding on these membranes; the only difference between these two cell systems were B_{max} values (38 vs. 2.4 pmol·mg^{-1} protein) and per cent non-specific/total binding (NSB/TB% of 1.3% vs. 11% respectively) that indicated a higher level of expression and lower NSB/TB% in HEK293 cells than that of CHO cells. However, since [^{3}H]EMPA binds to a single site in a saturable manner, the expression level of the receptor does not influence the determination of K_D. Hence, HEK293 cells were used for binding studies.

Antagonist potency and the inhibition mode of EMPA

In CHO(dHFr$^-$) cells stably expressing hOX_2 receptors, EMPA inhibited orexin-A- or orexin-B-evoked $[Ca^{2+}]_i$ response with IC_{50} = 8.8 ± 1.7 nmol·L^{-1}, n_H = 0.9 ± 0.0 and IC_{50} = 7.9 ± 1.7 nmol·L^{-1}, n_H = 1.0 ± 0.1 respectively (Figure 4). EMPA-mediated inhibition of orexin-A-induced $[Ca^{2+}]_i$ response was used to address further the selectivity of EMPA for hOX_2 over hOX_1 receptors in the functional assay. As seen in Figure 4, orexin-A-evoked $[Ca^{2+}]_i$ response was poorly inhibited by EMPA with IC_{50} > 10 000 nmol·L^{-1} in the CHO(dHFr$^-$)-hOX_1 stable cells.

To characterize the inhibition mode of EMPA, the concentration-response curves for [^{3}H]IP formation stimulated by orexin-A or orexin-B have been measured in the presence of various concentrations (0, 3, 10, 30, 100, 300 and 600 nmol·L^{-1}) of EMPA in the CHO(dHFr$^-$)-hOX_2 stable cell line. As seen in Figure 5A and C, orexin-A (0.03 nmol·L^{-1}–3 μmol·L^{-1}) and orexin-B (0.1 nmol·L^{-1}–10 μmol·L^{-1}) elicited concentration-dependent increases in the accumulation of [^{3}H]IP in the hOX_2 receptor expressing cells with the EC_{50}, n_H values of 1.1 ± 0.1 nmol·L^{-1}, 1.4 ± 0.1 and 2.4 ± 0.9 nmol·L^{-1}, 0.6 ± 0.1 respectively. EMPA behaved as a competitive antagonist at hOX_2 receptors, shifting both orexin-A and orexin-B concentration-response curves to the right without changing their maximal responses (Figure 5A and C). The apparent antagonist potency (pA_2) and the Schild slope values calculated from orexin-A and orexin-B Schild analyses (Figure 5B

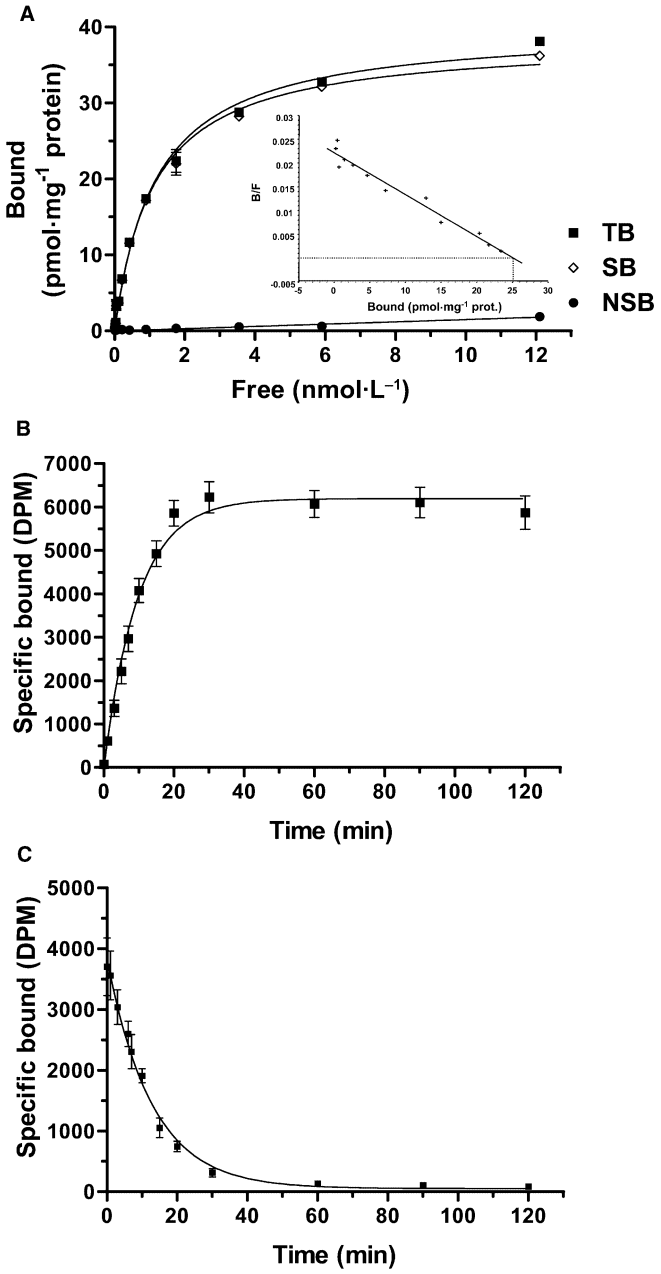

Figure 2 Binding characteristic of [^{3}H]EMPA to membrane preparations from HEK293 cells transiently expressing hOX_2 receptors. (A) Saturation binding curve and Scatchard plot (inset) of [^{3}H]EMPA binding to membranes from HEK293 cells transfected transiently with hOX_2 receptors. Specific binding (SB) was obtained by calculating the difference between total binding (TB) and non-specific binding (NSB), measured in the presence of 10 μmol·L^{-1} EMPA. Each data point is ±SEM (bars) of three individual experiments performed in triplicate. The data were analysed by non-linear regression analysis using GraphPad Prism 4.0 software and a single-site binding model. Time course for the association (B) and dissociation (C) of [^{3}H]EMPA binding to hOX_2 membranes. Each data point is ±SEM (bars) of three individual experiments, with four replicates.

and D) and are given in Table 3. As seen in Table 3, the functional potency of EMPA derived from FLIPR assay (pK_b) was in good agreement with that of the [^{3}H]IP accumulation assay (pA_2).

Selectivity profile of EMPA

The pharmacological specificity of EMPA was confirmed by assessment in radioligand binding assays in a broad CEREP screen (Paris, France) (http://www.cerep.fr) (Table 4). Among the 80 receptors in the CEREP broad screen, 30 were peptide receptors. For the selection of peptide receptors in this broad screen, the amino acids forming the transmembrane domains (7TMD) of human OX_2 receptors were aligned with those of the large number of peptide receptors in the protein database (Swissprot). The hOX_2 receptor 7TMD displayed a similarity of 37%, 29% and 23% to the 7TMD of $hNPY_2$ (neuropeptide Y2), $hCCK_1$ (cholesystokinin 1) and hNK_2 (neurokinin 2) receptors, respectively, and these classes of GPCRs were therefore included in our selectivity screen. EMPA was inactive (<50% activity at 10 μmol·L^{-1}) at all targets tested with the exception of the hV_{1a} (vasopressin) and KOP (κ opiate) receptors, where it caused 79% and 65%, respectively, displacement of specific binding at 10 μmol·L^{-1}. However, subsequent concentration-response curves with EMPA showed an IC_{50} = 5.75 μmol·L^{-1}, K_i = 2.63 μmol·L^{-1}, n_H = 1.0 and IC_{50} = 12.8 μmol·L^{-1}, K_i = 5.8 μmol·L^{-1}, n_H = 1.0 in the binding assay at human and mouse V_{1a} receptors respectively. EMPA also had K_i = 11.3 μmol·L^{-1}, n_H = 1.4 in the binding assay at hKOP. Hence, EMPA had negligible binding affinities at the human and mouse V_{1a} and hKOP receptors.

[^{3}H]EMPA binding to rat brain sections

The distribution and abundance of *in vitro* binding sites of [^{3}H]EMPA was investigated in coronal rat brain sections using autoradiography and image analysis (Figure 6). A high density of specific binding was observed in many brain regions including the limbic cortices, hippocampus, striatum and hypothalamic nuclei. NSB, determined in the presence of 10 μmol·L^{-1} Cp-5, a selective OX_2 receptor antagonist (Figure 6B) was <8% of TB.

Ex vivo receptor occupancy studies using [^{3}H]EMPA autoradiography

To further characterize the specificity of [^{3}H]EMPA binding in the rat brain, *ex vivo* binding experiment were conducted to investigate the ability of the known orexin antagonist almorexant to block the binding of [^{3}H]EMPA. Administration of almorexant (3, 10 or 30 mg·kg^{-1}, i.p.) resulted in a dose-dependent decrease of the binding of [^{3}H]EMPA to the cortical layer 6 (Figure 7A), hilus dentate gyrus (Figure 7B) and all other brain regions evaluated. These data provide a first estimation of OX_2 receptor occupancy produced by almorexant after systemic administration.

Physicochemical and pharmacokinetics properties of EMPA in mice and rats

The physicochemical properties of EMPA are: MW = 454.4 g·mol^{-1}; lipophilicity clogP/logD of 3.43/2.3 at pH 7.4; permeation coefficient $P_e = 5.5 \times 10^{-6}$ cm·s^{-1} (Parallel Artificial Membrane Permeation Assay, PAMPA); thermodynamic solubility of 278 μg·mL^{-1}; pK_a of 4.62 and a polar surface area of 73 Å^2. With the exception of 3A4, EMPA does not inhibit major

Table 1 Kinetic parameters for the association and dissociation of [^{3}H]EMPA in membrane preparations from HEK293 cells transiently expressing hOX_2 receptors

Compound	*Association kinetic*			*Dissociation kinetic*		*Apparent* K_D *nmol·L^{-1}*
	K_{ob} *min^{-1}*	K_{on} *nmol·L^{-1}·min^{-1}*	$t_{1/2}$ *min*	K_{off} *min^{-1}*	$t_{1/2}$ *min*	
[^{3}H]EMPA	0.11 ± 0.01	0.028 ± 0.06	6.29 ± 0.47	0.078 ± 0.00	8.89 ± 0.25	2.74 ± 0.20

The K_{ob} (observed on rate), K_{off} (observed off rate), K_{on} (calculated on rate), $t_{1/2}$ (half-maximal binding) and K_D (apparent dissociation constant) values are ±SEM, calculated from three independent experiments (each performed with four replicates) as described under *Methods*.

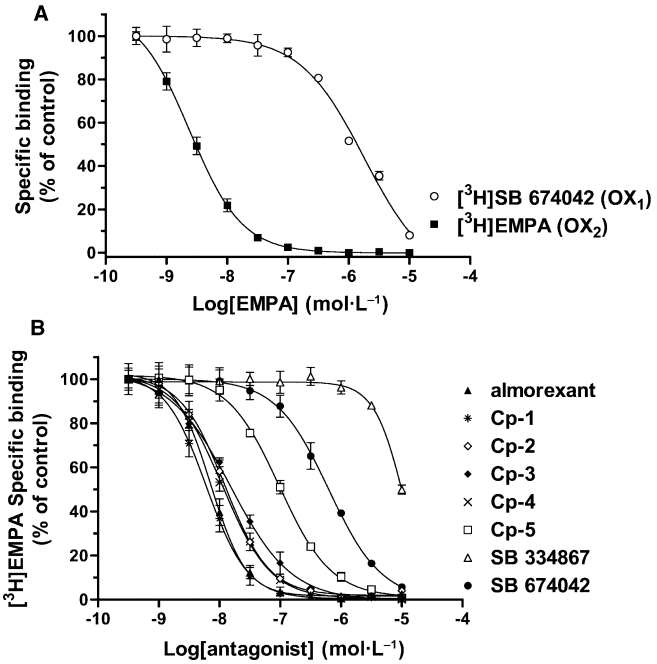

Figure 3 (A) The displacement of [^{3}H]SB 674042 and [^{3}H]EMPA binding by EMPA in membrane preparations from HEK293 cells transiently expressing hOX_1 and hOX_2 receptors respectively. (B) The displacement of [^{3}H]EMPA binding by OX_1-selective, OX_2-selective and dual OX_1/OX_2 receptor antagonists in the hOX_2 cell membrane. The [^{3}H]SB 674042 (0.7 nmol·L^{-1}) and [^{3}H]EMPA (1.1 nmol·L^{-1}) were used at a concentration equal to their K_D values in these competition binding experiments. Each data point is ±SEM (bars) of three individual experiments performed in duplicate.

Table 2 [^{3}H]EMPA displacement by various selective OX_1, OX_2 and dual OX_1/OX_2 receptor antagonists in the membrane preparations from HEK293 cells transiently expressing hOX_2 receptors

OX antagonists	K_i *nmol·L^{-1}*	n_H
EMPA	1.10 ± 0.24	1.01 ± 0.01
Almorexant	4.35 ± 0.27	1.22 ± 0.05
Cp-1	2.94 ± 0.66	1.27 ± 0.04
Cp-2	6.46 ± 0.60	1.18 ± 0.04
Cp-3	7.76 ± 0.50	0.87 ± 0.08
Cp-4	5.98 ± 0.51	1.10 ± 0.04
Cp-5	51.10 ± 3.44	1.02 ± 0.09
SB 334867	>10 000	
SB 674042	334.0 ± 110.0	1.0 ± 0.2

K_i and Hill slope (n_H) values for [^{3}H]EMPA binding inhibition by various antagonists were calculated as described under *Methods*. Values are ±SEM of the K_i calculated from three independent experiments, each performed in duplicate.

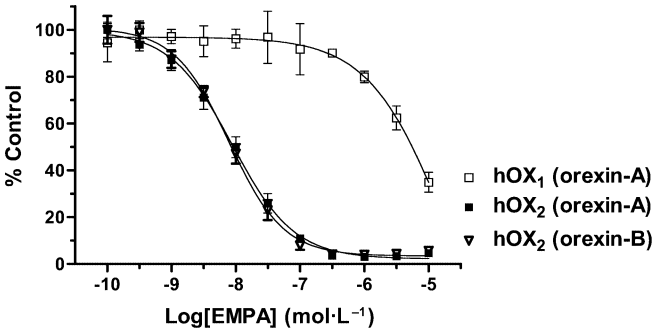

Figure 4 Inhibition of orexin induced Ca^{2+} mobilization by EMPA at hOX_1- and hOX_2-CHO-dHFr$^-$ stable cell lines. Concentration-dependent inhibition orexin-A and orexin-B stimulated increases in $[Ca^{2+}]_i$ by EMPA as assayed using the Ca^{2+}-sensitive dye, Flou-4 and a Fluorometric Imaging Plate Reader (FLIPR-96). Each curve represents ±SEM (bars) of the three dose-response measurements (each performed in duplicate).

cytochrome P450 isoenzymes (human liver microsomes IC_{50} values: 3A4: 0.7 μmol·L^{-1}; 2D6 and 2C9: >50 μmol·L^{-1}). EMPA displayed a weak activity as a substrate for P-glycoprotein mediated efflux transport. Furthermore, EMPA inhibited human ERG channel with an IC_{50} value of 3.6 μmol·L^{-1} (27% at 1 μmol·L^{-1}, 69% at 10 μmol·L^{-1}).

The oral bioavailability and pharmacokinetics of EMPA were evaluated in male NMRI mice and Wistar rats. The mean pharmacokinetic parameters of EMPA after single intravenous (i.v.) or oral (p.o.) bolus administration in mice and rat are given in Table 5. The concentration of EMPA in rat brain measured at 2 and 4 h was <10 ng·mL^{-1}. EMPA is highly protein bound (2.8%, 4.7% and 10% free fraction in human, mouse and rat plasma respectively). The stability of EMPA measured 1 h/4 h in human, mouse and rat plasma was 133%/96%, 105%/109% and 136%/135% respectively.

Monitoring of EMPA exposure in mice and rats at the completion of the behavioural procedures

To determine EMPA exposure, plasma and brain exposure of EMPA were monitored at the end of the behavioural procedures mentioned below in mice and rats. In the reversal of [Ala^{11},D-Leu^{15}]orexin-B-induced hyperlocomotion test in mice, the plasma concentrations, measured 45 min after i.p. injection of EMPA at doses 30, 100 and 300 mg·kg^{-1} were 73, 2182 and 23 300 ng·mL^{-1} respectively. The brain level of EMPA, given at a dose of 300 mg·kg^{-1} and measured 45 min after i.p. injection was 16 419 ng·mL^{-1}. In the rat LMA test, the plasma levels of EMPA, given at doses of 3, 10 and

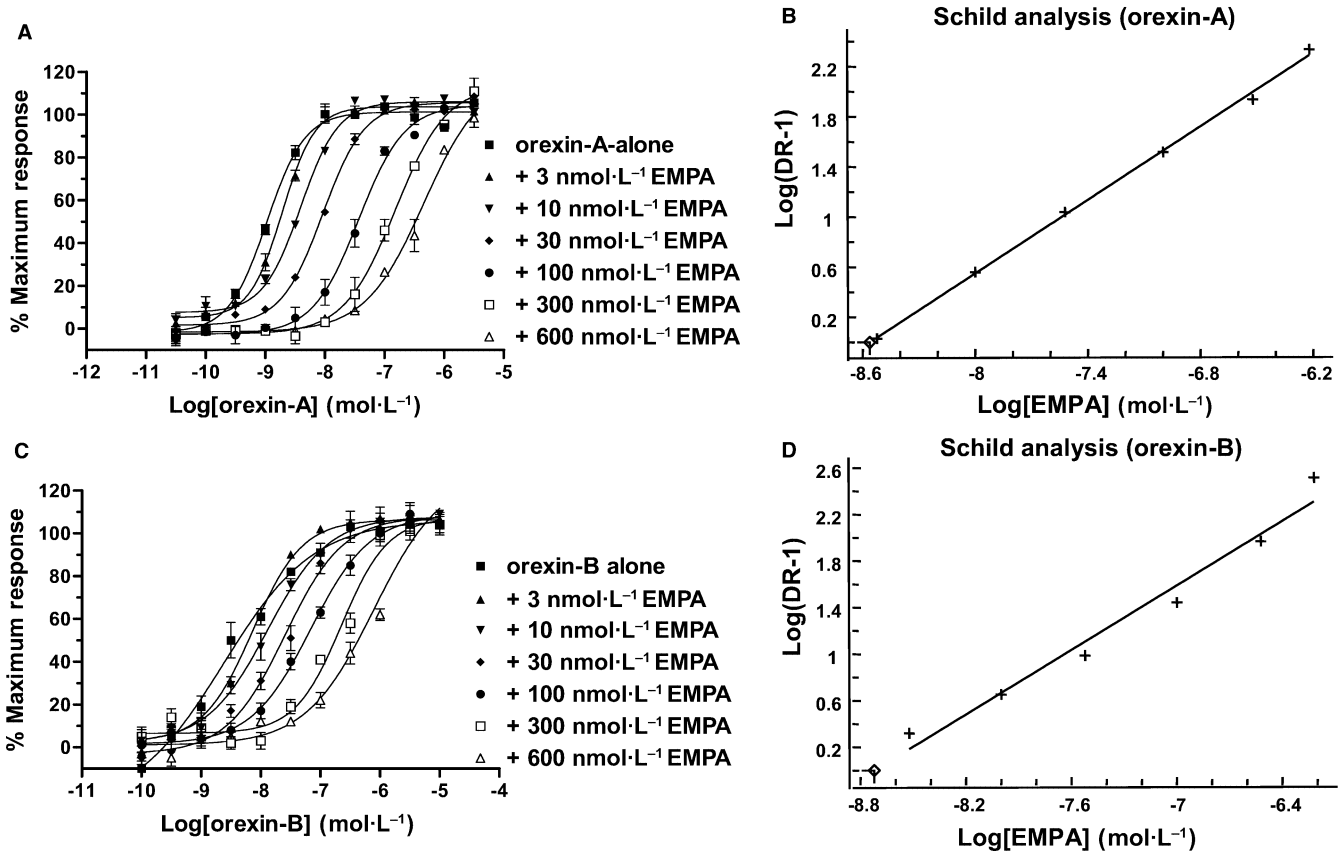

Figure 5 Schild analyses showing the competitive mode of antagonism by EMPA at OX_2 receptors. Concentration-response curves for [^{3}H]IP formation stimulated by orexin-A (A) and orexin-B (C) in the absence and presence of various concentrations of EMPA in CHO(dHFr$^-$)-hOX_2 stable cell line. Schild plots for antagonism by EMPA (B and D). The EC_{50} and EC_{50}′ values, which derived from orexin-A and orexin-B concentration-response curves in the absence and presence of increasing fixed concentrations of EMPA (A and C), were used to calculate the dose ratios (DR = EC_{50}′/EC_{50}) and plotted according to Schild regression in panels b and d. Each concentration-response curve is ±SEM (bars) of three individual experiments, each performed with four replicates.

Table 3 Antagonism profile of EMPA as analysed in FLIPR and Schild plot

	$[Ca^{2+}]_i$ mobilization			*Schild analysis*		
	pK_b	*K_b nmol·L^{-1}*	*n_H*	*pA_2*	*$K_b{}^a$ nmol·L^{-1}*	*Schild slope*
Orexin-A	9.1	0.8 ± 0.2	0.9 ± 0.0	8.6	2.8	1.0
Orexin-B	9.2	0.6 ± 0.0	1.0 ± 0.1	8.8	1.6	0.9

pK_b, K_b and Hill coefficient (n_H) values for the inhibition of orexin-A- or orexin-B-evoked $[Ca^{2+}]_i$ response in the CHO(dHFr$^-$)-hOX_2 receptor stable cell line were calculated as described under Methods. Data are ±SEM of the three dose-response measurements (each performed in duplicate). Schild constants for antagonism of orexin-A- or orexin-B-induced accumulation of [^{3}H]IP by EMPA in the CHO(dHFr$^-$)-hOX_2 cells. The apparent antagonist potency (pA_2) and Schild slope values of EMPA were determined from Schild plot analyses shown in Figure 5B and D.

30 mg·kg^{-1}and determined 65 min after i.p. injection were 7, 32 and 68 ng·mL^{-1} respectively. However, the brain level of EMPA (30 mg·kg^{-1}) in rats, measured 65 min after i.p. dosing, was approximately 8 ng·mL^{-1}.

In vivo activity of EMPA

Reversal of [Ala^{11},D-Leu^{15}]orexin-B-induced hyperlocomotion in mice

As shown on Figure 8, and as compared with animals injected with artificial CSF (open symbol), mice given 3 μg of the preferential OX_2 receptor agonist [Ala^{11},D-Leu^{15}]orexin-B i.c.v. exhibited marked increases in LMA (>300%). EMPA (1, 3, 10, 30, 100, 300 mg·kg^{-1} i.p.) dose-dependently reversed this [Ala^{11},D-Leu^{15}]orexin-B-induced hyperlocomotion [$F(6,49) = 15.1$, $P < 0.001$] without itself significantly affecting LMA [$F(6,41) = 1.12$, $P > 0.05$].

Spontaneous locomotor activity in rats during the dark (active) phase

When placed in the activity monitoring chambers, vehicle-treated animals initially exhibited a marked hyperactivity

Table 4 CEREP selectivity screen in the broad radioligand binding assays were undertaken to determine the pharmacological activity of EMPA

Target	*Reference compound*	*% control (10 µmol·L^{-1}) mean SB*	*Target*	*Reference compound*	*% control (10 µmol·L^{-1}) mean SB*
A_1 (h)	DPCPX	82	M_4 (h)	4-DAMP	107
A_{2A} (h)	NECA	95	M_5 (h)	4-DAMP	98
A_3 (h)	IB-MECA	106	NK_1 (h)	[Sar9,Met(O2)11]-SP	109
α_1 (non-selective)	Prazosin	102	NK_2 (h)	[Nle10]-NKA(4-10)	93
α_2 (non-selective)	Yohimbine	92	NK_3 (h)	SB 222200	82
β_1 (h)	Atenolol	97	Y_1 (h)	NPY	110
β_2 (h)	ICI 118551	99	Y_2 (h)	NPY	97
AT_1 (h)	Saralasin	101	NT_1 (h) (NTS1)	Neurotensin	98
AT_2 (h)	Saralasin	104	Delta 2 (h) (DOP)	DPDPE	105
BZD (central)	Diazepam	84	Kappa (KOP)	U 50488	**30**
BZD (peripheral)	PK 11195	70	mu (h) (MOP) (agonist site)	DAMGO	91
BB (non-selective)	Bombesin	77	ORL1 (h) (NOP)	Nociceptin	115
B_2 (h)	NPC 567	93	PACAP (h) (PAC1)	PACAP1-38	101
CGRP (h)	hCGRPalpha	132	PCP	MK 801	101
CB_1 (h)	CP 55940	94	TXA2/PGH2 (h) (TP)	U 44069	73
CCK_A (h) (CCK_1)	CCK-8	97	P2X	Alpha, beta-MeATP	110
CCK_B (h) (CCK_2)	CCK-8	95	P2Y	dATPalpha S	89
D_1 (h)	SCH 23390	99	5-HT_{1A} (h)	8-OH-DPAT	98
D_{2S} (h)	(+)butaclamol	95	5-HT_{1B} (h)	Serotonin	95
D_3 (h)	(+)butaclamol	101	5-HT_{2A} (h)	Ketanserin	89
$D_{4.4}$ (h)	Clozapine	95	5-HT_{2C} (h)	RS-102221	81
D_5 (h)	SCH 23390	97	5-HT_3 (h)	MDL 72222	103
ET_A (h)	Endothelin-1	99	5-HT_{5A} (h)	Serotonin	100
ET_B (h)	Endothelin-3	95	5-HT_6 (h)	Serotonin	92
GABA (non-selective)	GABA	107	5-HT_7 (h)	Serotonin	98
GAL_1 (h)	Galanin	96	Sigma (non-selective)	Haloperidol	106
GAL_2 (h)	Galanin	100	sst (non-selective)	Somatostatin-14	97
PDGF	PDGF BB	94	VIP1 (h) (VPAC1)	VIP	104
CXCR2 (h) (IL-8B)	IL-8	101	V_{1a} (h)	[d(CH2)51,Tyr(Me)2]-AVP	**21**
TNF-alpha (h)	TNF-alpha	93	Ca^{2+} channel (L, verapamil site) (phenylalkylamines)	D 600	108
CCR1 (h)	MIP-1alpha	101			
H_1 (h)	Pyrilamine	106	K + V channel	Alpha-dendrotoxin	98
H_2 (h)	Cimetidine	93	SK + Ca channel	Apamin	89
MC_4 (h)	NDP-alpha-MSH	103	Na^+ channel (site 2)	Veratridine	100
MT_1 (h)	Melatonin	59	Cl^- channel	Picrotoxinin	94
M_1 (h)	Pirenzepine	83	NE transporter (h)	Protriptyline	106
M_2 (h)	Methoctramine	93	DA transporter (h)	BTCP	71
M_3 (h)	4-DAMP	95	5-HT transporter (h)	Imipramine	108

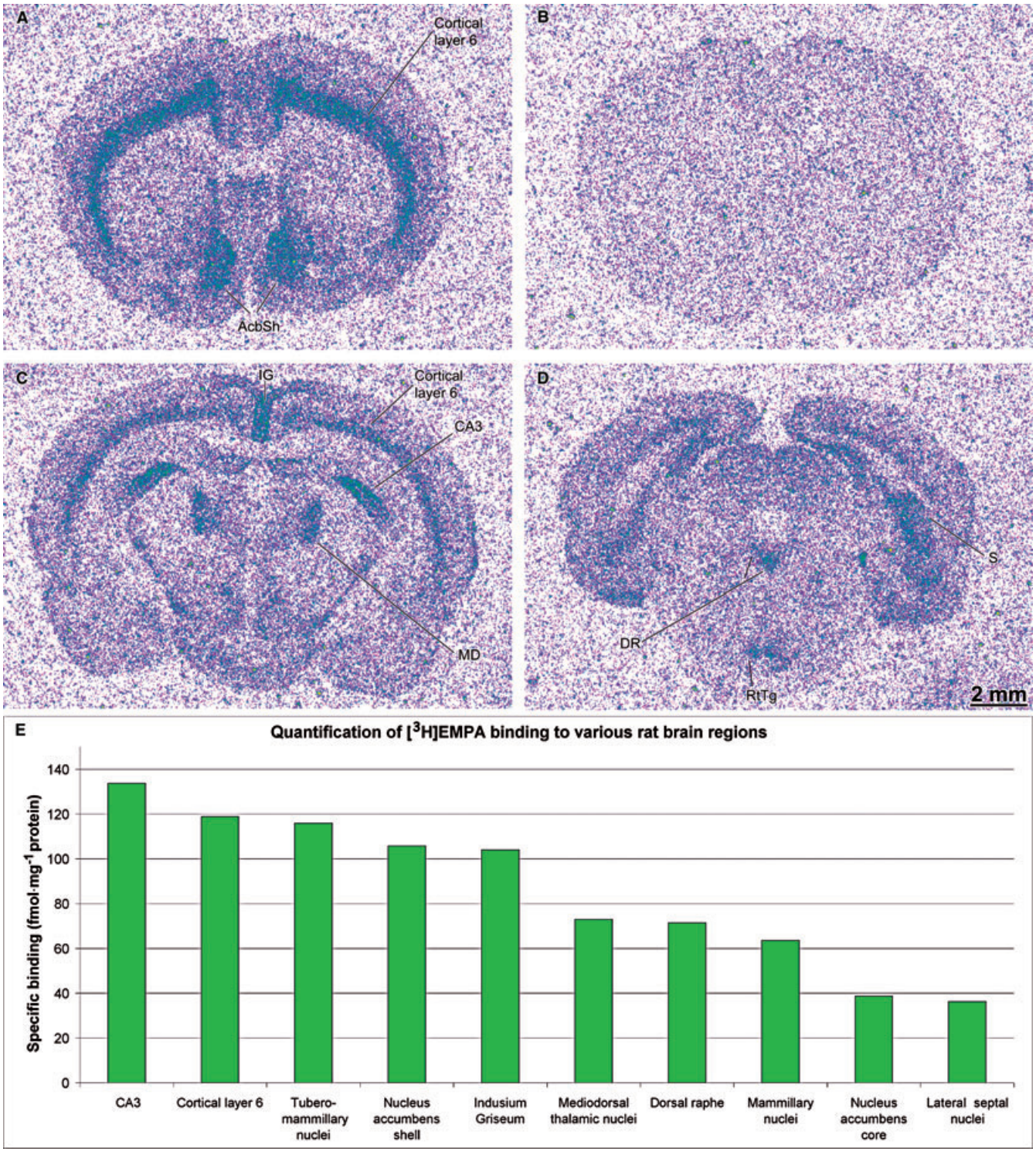

Figure 6 Regional distribution of [^{3}H]EMPA binding sites in coronal sections of rat brain revealed by autoradiography. Panel A, C and D show total binding (1 nmol·L^{-1} [^{3}H]EMPA); B shows non-specific binding (+10 µmol·L^{-1} Cp-5); (E) Regional abundance of [^{3}H]EMPA specific binding (1 nmol·L^{-1}) measured by quantitative autoradiography and image analysis. Mean values are expressed as fmol mg^{-1} protein. Competition with 10 µmol·L^{-1} Cp-5, no binding is evident (panel B). Abbreviations used in the figure: AcbSh, nucleus accumbens shell; IG, indusium griseum; CA3 region of the hippocampus; MD mediodorsal thalamic nuclei; DR, dorsal raphe nucleus; S, subiculum; RtTg, reticulotegmental neuclei of the pons.

that rapidly adapted over the 30 min recording period. In drug-treated animals, EMPA (3, 10, 30 mg·kg^{-1} i.p.) induced a significant and dose-dependent reduction in the baseline LMA [$F(3,28) = 5.24$, $P < 0.01$; Figure 9]. This decrease in locomotion was already evident 5 min after giving the 10 and 30 mg·kg^{-1} doses. When activity was summated over a 10 min period (the inset in top-right corner of Figure 9), EMPA demonstrated a clear dose-dependent inhibition of spontaneous

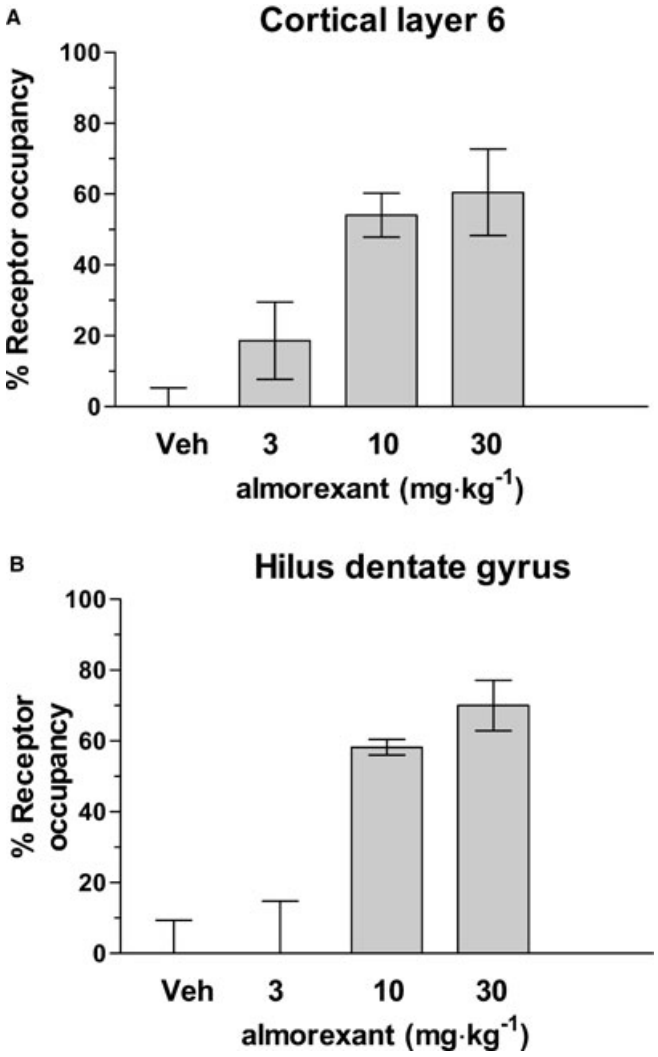

Figure 7 OX_2 receptor occupancy by almorexant (3, 10, 30 mg·kg^{-1} i.p.) in the rat cortical layer 6 (A) and hilus dentate gyrus (B) determined using *ex vivo* [^{3}H]EMPA autoradiography.

activity as compared with vehicle-treated animals [$F(3,28) = 4.18$, $P < 0.05$].

Motor coordination and balance in rats

In the rotarod test, no significant motor disturbances were observed following treatment with EMPA (3, 10 and 30 mg·kg^{-1} i.p.) when animals were examined on a bar rotating at 8 r.p.m. [$F(3,28) = 0.71$, $P > 0.05$] or 16 r.p.m. [$F(3,28) = 0.59$, $P > 0.05$], as shown in Figure 10.

Discussion

The orexin system and OX_2 receptors may play a role in stress and in the regulation of emotional responses via its interaction with the corticotropin releasing factor (CRF) system in the hypothalamus (Sakamoto *et al.*, 2004). I.c.v. injection of orexin-A induces grooming (stress response) that is blocked in part by a CRF antagonist (Ida *et al.*, 2000). OX_2 receptors are predominantly expressed in the paraventricular nucleus in the hypothalamus and orexin neurons projecting to CRF neurons express mainly OX_2 receptors (Winsky-Sommerer *et al.*, 2004; 2005). Therefore, OX_2 receptor stimulation activates the hypothalamo-pituitary-adrenal axis. Interestingly, a recent study has also shown that a selective OX_2 receptor antagonist, N-{(1S)-1-(6,7-dimethoxy-3,4-dihydro-2(1H)-isoquinolinyl)carbonyl}-2,2-dimethylpropyl)-N-amine, was able to attenuate the orexin-A-induced increases in plasma ACTH (Chang *et al.*, 2007). Thus far, however, there are few reports describing biochemical and pharmacological characterization of selective OX_2 receptor antagonists. Here, we describe the *in vitro* and *in vivo* properties of a highly selective OX_2 receptor antagonist, EMPA.

[^{3}H]EMPA binds to a single saturable site on recombinantly expressed human and rat OX_2 receptors (B_{max} of 38.29 ± 0.50 and 6.62 ± 0.60 pmol·mg^{-1} protein respectively) with high affinity (K_D values of 1.11 ± 0.05 nmol·L^{-1} and 1.36 ± 0.04 nmol·L^{-1} respectively). Similarly, EMPA was able to displace the [^{3}H]EMPA binding from cell membranes containing human and rat OX_2 receptors, with K_i values of 1.10 ± 0.24 nmol·L^{-1} and 1.45 ± 0.13 nmol·L^{-1} and Hill values of 1.01 ± 0.01 and 0.93 ± 0.08 respectively. At the K_D value, NSB for [^{3}H]EMPA was approximately 1.3% of total bound radioactivity. EMPA displayed a high selectivity (900-fold in binding and >10 000-fold in FLIPR assays) for OX_2 over OX_1 receptors. Moreover, the selective OX_2 and dual OX_1/OX_2 receptor antagonists were able to competitively displace [^{3}H]EMPA binding from hOX$_2$-HEK293 membranes with the following rank order of potency: EMPA > Cp-1 > almorexant > Cp-4 > Cp-2 > Cp-3 > Cp-5. The selective OX_1 receptor antagonists, SB 334867 and SB 674042 only poorly displaced [^{3}H]EMPA binding from OX_2-HEK293 membranes (K_i values >10 000 and 334 nmol·L^{-1} respectively).

In functional studies, EMPA inhibited orexin-A- and orexin-B-induced $[Ca^{2+}]_i$ responses in a CHO(dHFr$^-$)-hOX$_2$ stable cell line with a K_b value of 0.8 or 0.6 nmol·L^{-1} respectively. Analysis of the antagonism by EMPA, using orexin-A- or orexin-B-evoked accumulation of [^{3}H]IP assay in CHO(dHFr$^-$)-hOX$_2$ cells, revealed that it behaved as a competitive antagonist with a Schild slope close to unity. Therefore, EMPA antagonized orexin-A and orexin-B with similar potency in hOX$_2$ receptor expressing cells and there was a good correlation between EMPA's affinity constant (K_i) and apparent antagonist potency (K_b^a). Moreover, EMPA was assessed over a battery of 80 different binding sites that included numerous other GPCRs, transporters and ion channels. The results obtained indicate that EMPA displays a high degree of selectivity for OX_2 receptors

The property of the radioligand [^{3}H]EMPA to selectively bind *in vitro* to rat brain sections was investigated. This study is the first to describe the regional binding properties of a radiolabelled selective antagonist for OX_2 receptors in rat brain. High density of specific binding was observed in the CA3 region of the hippocampus, cortical layer 6, tuberomammillary nucleus, induseum griseum and nucleus accumbens. Binding was also observed in various thalamic and hypothalamic nuclei known to express OX_2 receptors, such as the dorsal raphe and the pontine gray. Binding of [^{3}H]EMPA to brain sections was completely abolished by the addition of

Table 5 Pharmacokinetic assessment of EMPA after i.v. and p.o. administration to mice and rats

Route	*Mouse*				*Rat*	
	Plasma		*Brain*		*Plasma*	
	i.v.	*p.o.*	*i.v.*	*p.o.*	*i.v.*	*p.o.*
Dose, $mg \cdot kg^{-1}$	10.77	18.04	10.77	18.04	11.79	19.71
C_{max}/dose, $ng \cdot mL^{-1}$	512.1	68.2	266.2	13.7	421.9	1.8
T_{max}, h	0	0.5	0	0.25	0	0.63
AUC/dose, $ng \cdot h \cdot mL^{-1}$	201.4	43.7	56.3	7.3	127.4	1.4
$T_{1/2}$, h	1.85	0.98	0.15	0.14	0.81	0.37
Vss, $L \cdot kg^{-1}$	1.31		2.71		2.07	
CL, $mL \cdot min^{-1} \cdot kg^{-1}$	82.8		295.8		131.7	
F, %		21.7				1.1
Fu, %		4.7				10.0

C_{max}, maximum concentration; T_{max}, time at which maximum concentration was observed; AUC, area under the plasma concentration versus time curve; CL, clearance; Vss, volume of distribution at steady state; $T_{1/2}$, terminal half-life; F, bioavailability; Fu, fraction unbound. Values are means for mice ($n = 2$ per time point) and for rats ($n = 2$).

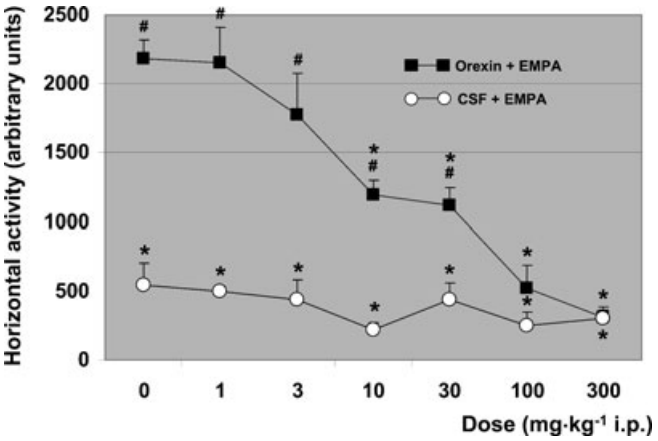

Figure 8 Effects of EMPA (0, 1, 3, 10, 30, 100, 300 $mg \cdot kg^{-1}$ i.p.) on [Ala^{11},D-Leu^{15}]orexin-B-induced hyperlocomotion (orexin + EMPA) and spontaneous locomotor activity (CSF + EMPA) in mice. Data points indicate mean horizontal activity counts per group, error bars indicate SEM ($n = 8$ per group). # indicates significant difference from vehicle/CSF group, and asterisks indicate significant difference from orexin/vehicle group in *post hoc* testing ($P < 0.05$ at least).

the non-radiolabelled dual antagonist, almorexant, or selective OX_2 receptor antagonists (CP-5 and EMPA). The *ex vivo* [^{3}H]EMPA binding studies allowed determination of OX_2 receptor occupancy by almorexant in rat brain regions. When given i.p., almorexant dose-dependently increased OX_2 receptor occupancy, as measured by displacement of [^{3}H]EMPA, with a dose of 30 $mg \cdot kg^{-1}$ producing 60–70% occupancy in rat brain. These results confirm the selectivity of [^{3}H]EMPA for OX_2 receptors. Furthermore, the distribution of binding sites for [^{3}H]EMPA in coronal sections of rat brain were in good correlation with that of OX_2 receptor transcripts and protein studied by hybridization histochemistry (Trivedi *et al.*, 1998; Marcus *et al.*, 2001) and IHC (Cluderay *et al.*, 2002). The high density of [^{3}H]EMPA binding in cortical layer 6 is in good agreement with a previous report showing the exclusive postsynaptic excitatory action of orexin on sublayer 6b cortical neurons via its interaction with OX_2 receptors (Bayer *et al.*, 2004). It is interesting to note that the highest binding density in the nucleus accumbens was observed in the shell yet only moderate binding in the core. In this context, the lateral hypothalamic orexin neurons project to reward-associated brain regions that include the nucleus accumbens and the ventral tegmental area suggesting the involvement of orexins in drug-seeking and other motivational behaviours (Harris *et al.*, 2005; Scammell and Saper, 2005). Indeed, the infusion of orexin-A into the nucleus accumbens shell in rat stimulated both feeding and LMA (Thorpe and Kotz, 2005) while the preadministration of SB-334867-A (an OX_1 receptor selective antagonist) significantly attenuated this orexin-A-induced feeding activity but had no effect on orexin-A-augmented LMA. As OX_2 receptors are expressed in nucleus accumbens to a greater extent than are OX_1 receptors (Lu *et al.*, 2000; Cluderay *et al.*, 2002), it is plausible that the effects on LMA are mediated via OX_2 receptors. Furthermore, it has recently been shown that orexin-A activation of the nucleus accumbens shell acted as a mediator in the expression of precipitated morphine withdrawal (Sharf *et al.*, 2008).

The single-dose pharmacokinetic profiles of EMPA were assessed in mice and rats after intravenous and oral administration. EMPA displayed a high systemic plasma clearance, medium volume of distribution at steady state and low oral bioavailability in both mouse and rat. The mean brain/plasma concentration ratio of EMPA (at dose of 18 $mg \cdot kg^{-1}$, p.o.) was 0.2 in mouse. Because of lower oral bioavailability of EMPA in rat (F = 1.1%) in comparison to mouse (F = 21.7%), the brain level of EMPA in rat (at dose of 20 $mg \cdot kg^{-1}$, p.o.) was <10 $ng \cdot mL^{-1}$. Moreover, the plasma and brain exposure of EMPA was evaluated at the end of rodent behavioural procedures: the mean brain/plasma concentration ratios of EMPA determined at 45 and 65 min after i.p. administration were 0.7 and 0.1 in mouse and rat respectively.

Orexin levels fluctuated diurnally in freely moving rats with levels slowly increasing during active phase and decreased during the rest (Taheri *et al.*, 2000; Yoshida *et al.*, 2001; Desarnaud *et al.*, 2004). Moreover, i.c.v. injection of orexin-A during the resting phase increased arousal, grooming and LMA (Ida *et al.*, 2000; Nakamura *et al.*, 2000; Piper

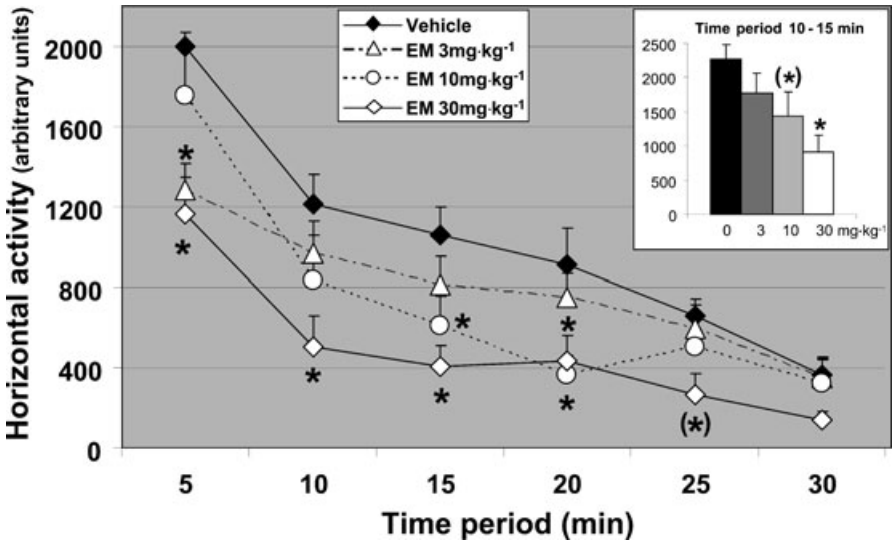

Figure 9 Effects of EMPA (3, 10, 30 mg·kg^{-1} i.p.) on spontaneous locomotor activity in rat. Each data point indicates mean horizontal activity counts per 5 min time period; error bars indicate SEM (n = 8 per group). The bar chart in the inset depicts the dose-dependent effect of the compound on cumulative horizontal activity over the time period 10–15 min. Asterisks indicate significant difference from vehicle-treated group in *post hoc* testing ($P < 0.05$ at least).

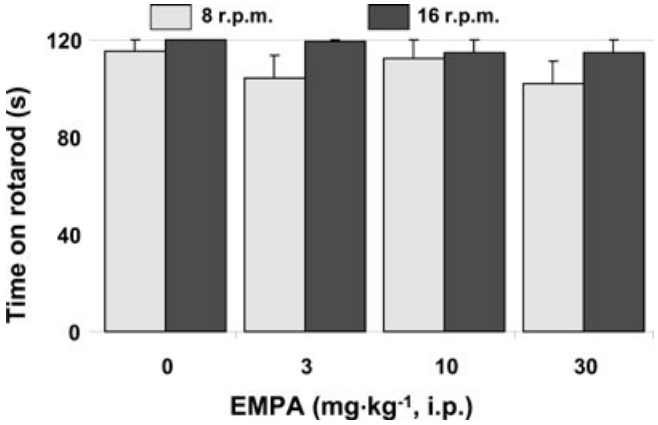

Figure 10 Rotarod performance following injection of 3, 10 or 30 mg·kg^{-1} i.p. of EMPA compared to vehicle controls. Bars indicate mean time spent on rotarod in seconds (maximum 120 s) ± SEM.

et al., 2000). In the present study, a selective OX_2 receptor agonist, [Ala^{11},D-Leu^{15}]orexin-B, which had shown a 400-fold selectivity for the OX_2 (EC_{50} = 0.13 nmol·L^{-1}) over OX_1 receptors (EC_{50} = 52 nmol·L^{-1}) (Asahi *et al.*, 2003) was used to better address EMPA's selectivity for OX_2 receptors *in vivo*. During the resting phase, i.c.v. injection of [Ala^{11},D-Leu^{15}]orexin-B in mice significantly induced hyperlocomotor activity relative to vehicle. Although EMPA by itself had no effect on spontaneous LMA in freely moving mice, it significantly reversed [Ala^{11},D-Leu^{15}]orexin-B-induced hyperlocomotion in a dose-dependent manner during the resting phase. Furthermore, EMPA, given in rats during the active phase, reduced significantly the LMA in a dose-dependent manner. Of note was the significant inhibition in spontaneous activity, compared with the vehicle treated animal, when LMA was summated over a 10 min period after 30 mg·kg^{-1} i.p. administration of EMPA, this despite a low brain to plasma ratio of EMPA and limited bioavailability in rat. As the OX_2 receptor is expressed at a low level in rat peripheral tissues (Voisin *et al.*, 2003; Heinonen *et al.*, 2008) and anatomical, neurochemical and behavioural studies in rodents all support a central role of endogenous orexin in regulating motor activity (Peyron *et al.*, 1998; Piper *et al.*, 2000; Baldo *et al.*, 2003; Krout *et al.*, 2003), the observed cerebral level of 8 ng·mL^{-1} that is equivalent to a 18 nmol·L^{-1} concentration or more precisely 1.8 nmol·L^{-1} unbound EMPA in rat brain was nevertheless sufficient to exert this effect centrally, due to EMPA's high potency (K_b = 0.6 nmol·L^{-1}) and fraction unbound (Fu = 10%). However, EMPA did not induce any deficits in the rat rotarod performance procedure for motor coordination and balance. The robust activity of EMPA in reversal of hyperlocomotion induced by a selective OX_2 receptor agonist further substantiates the *in vivo* selectivity of EMPA for the OX_2 receptor that is in good agreement with the high degree of selectivity observed *in vitro*. In conclusion, EMPA is a high-affinity, reversible, selective and *in vivo* active OX_2 receptor antagonist. Thus, EMPA could prove useful when investigating the role played by OX_2 receptors in pathophysiological processes of CNS disorders such as insomnia, cluster headache, drug abuse and maladaptation to stress.

Acknowledgements

We are grateful to Patricia Glaentzlin, Valérie Goetschy, Claudia Kratzeisen, Anne Marcuz, Marie-Thérèse Miss, Céline Sutter and Marie-Thérèse Zenner for their excellent technical assistance.

Conflicts of interest

All authors are employees of F. Hoffmann-La Roche Ltd.

References

Alexander SPH, Mathie A, Peters JA (2008). Guide to receptors and channels (GRAC), 3rd edn. *Br J Pharmacol* **153** (Suppl. 2): S1–S209.

Asahi S, Egashira S, Matsuda M, Iwaasa H, Kanatani A, Ohkubo M *et al*. (2003). Development of an orexin-2 receptor selective agonist, [Ala(11), D-Leu(15)]orexin-B. *Bioorg Med Chem Lett* **13**: 111–113.

Baldo BA, Daniel RA, Berridge CW, Kelley AE (2003). Overlapping distributions of orexin/hypocretin- and dopamine-beta-hydroxylase immunoreactive fibers in rat brain regions mediating arousal, motivation, and stress. *J Comp Neurol* **464**: 220–237.

Bayer L, Serafin M, Eggermann E, Saint-Mleux B, Machard D, Jones BE *et al*. (2004). Exclusive postsynaptic action of hypocretin-orexin on sublayer 6b cortical neurons. *J Neurosci* **24**: 6760–6764.

Brisbare-Roch C, Dingemanse J, Koberstein R, Hoever P, Aissaoui H, Flores S *et al*. (2007). Promotion of sleep by targeting the orexin system in rats, dogs and humans. *Nat Med* **13**: 150–155.

Chang H, Saito T, Ohiwa N, Tateoka M, Deocaris CC, Fujikawa T *et al*. (2007). Inhibitory effects of an orexin-2 receptor antagonist on orexin A- and stress-induced ACTH responses in conscious rats. *Neurosci Res* **57**: 462–466.

Chemelli RM, Willie JT, Sinton CM, Elmquist JK, Scammell T, Lee C *et al*. (1999). Narcolepsy in orexin knockout mice: molecular genetics of sleep regulation. *Cell* **98**: 437–451.

Cluderay JE, Harrison DC, Hervieu GJ (2002). Protein distribution of the orexin-2 receptor in the rat central nervous system. *Regul Pept* **104**: 131–144.

de Lecea L, Kilduff TS, Peyron C, Gao X, Foye PE, Danielson PE *et al*. (1998). The hypocretins: hypothalamus-specific peptides with neuroexcitatory activity. *Proc Natl Acad Sci USA* **95**: 322–327.

Desarnaud F, Murillo-Rodriguez E, Lin L, Xu M, Gerashchenko D, Shiromani SN *et al*. (2004). The diurnal rhythm of hypocretin in young and old F344 rats. *Sleep* **27**: 851–856.

Harris GC, Wimmer M, Aston-Jones G (2005). A role for lateral hypothalamic orexin neurons in reward seeking. *Nature* **437**: 556–559.

Heinonen MV, Purhonen AK, Makela KA, Herzig KH (2008). Functions of orexins in peripheral tissues. *Acta Physiol (Oxf)* **192**: 471–485.

Hirose M, Egashira S, Goto Y, Hashihayata T, Ohtake N, Iwaasa H *et al*. (2003). N-acyl 6,7-dimethoxy-1,2,3,4-tetrahydroisoquinoline: the first orexin-2 receptor selective non-peptidic antagonist. *Bioorg Med Chem Lett* **13**: 4497–4499.

Holland P, Goadsby PJ (2007). The hypothalamic orexinergic system: pain and primary headaches. *Headache* **47**: 951–962.

Huang ZL, Qu WM, Li WD, Mochizuki T, Eguchi N, Watanabe T *et al*. (2001). Arousal effect of orexin A depends on activation of the histaminergic system. *Proc Natl Acad Sci USA* **98**: 9965–9970.

Ida T, Nakahara K, Murakami T, Hanada R, Nakazato M, Murakami N (2000). Possible involvement of orexin in the stress reaction in rats. *Biochem Biophys Res Commun* **270**: 318–323.

Krout KE, Mettenleiter TC, Loewy AD (2003). Single CNS neurons link both central motor and cardiosympathetic systems: a double-virus tracing study. *Neuroscience* **118**: 853–866.

Langmead CJ, Jerman JC, Brough SJ, Scott C, Porter RA, Herdon HJ (2004). Characterisation of the binding of [3H]-SB-674042, a novel nonpeptide antagonist, to the human orexin-1 receptor. *Br J Pharmacol* **141**: 340–346.

Lin L, Faraco J, Li R, Kadotani H, Rogers W, Lin X *et al*. (1999). The sleep disorder canine narcolepsy is caused by a mutation in the hypocretin (orexin) receptor 2 gene. *Cell* **98**: 365–376.

Lu XY, Bagnol D, Burke S, Akil H, Watson SJ (2000). Differential distribution and regulation of OX1 and OX2 orexin/hypocretin receptor messenger RNA in the brain upon fasting. *Horm Behav* **37**: 335–344.

Malherbe P, Kratochwil N, Muhlemann A, Zenner MT, Fischer C, Stahl M *et al*. (2006). Comparison of the binding pockets of two chemically unrelated allosteric antagonists of the mGlu5 receptor and identification of crucial residues involved in the inverse agonism of MPEP. *J Neurochem* **98**: 601–615.

Marcus JN, Aschkenasi CJ, Lee CE, Chemelli RM, Saper CB, Yanagisawa M *et al*. (2001). Differential expression of orexin receptors 1 and 2 in the rat brain. *J Comp Neurol* **435**: 6–25.

Nakamura T, Uramura K, Nambu T, Yada T, Goto K, Yanagisawa M *et al*. (2000). Orexin-induced hyperlocomotion and stereotypy are mediated by the dopaminergic system. *Brain Res* **873**: 181–187.

Nambu T, Sakurai T, Mizukami K, Hosoya Y, Yanagisawa M, Goto K (1999). Distribution of orexin neurons in the adult rat brain. *Brain Res* **827**: 243–260.

Nishino S (2007). The hypocretin/orexin receptor: therapeutic prospective in sleep disorders. *Expert Opin Investig Drugs* **16**: 1785–1797.

Nishino S, Ripley B, Overeem S, Lammers GJ, Mignot E (2000). Hypocretin (orexin) deficiency in human narcolepsy. *Lancet* **355**: 39–40.

Ohno K, Sakurai T (2008). Orexin neuronal circuitry: role in the regulation of sleep and wakefulness. *Front Neuroendocrinol* **29**: 70–87.

Peyron C, Faraco J, Rogers W, Ripley B, Overeem S, Charnay Y *et al*. (2000). A mutation in a case of early onset narcolepsy and a generalized absence of hypocretin peptides in human narcoleptic brains. *Nat Med* **6**: 991–997.

Peyron C, Tighe DK, van den Pol AN, de Lecea L, Heller HC, Sutcliffe JG *et al*. (1998). Neurons containing hypocretin (orexin) project to multiple neuronal systems. *J Neurosci* **18**: 9996–10015.

Piper DC, Upton N, Smith MI, Hunter AJ (2000). The novel brain neuropeptide, orexin-A, modulates the sleep-wake cycle of rats. *Eur J Neurosci* **12**: 726–730.

Rainero I, Gallone S, Rubino E, Ponzo P, Valfre W, Binello E *et al*. (2008). Haplotype analysis confirms the association between the HCRTR2 gene and cluster headache. *Headache* **48**: 1108–1114. Epub 2008 Apr 8.

Rainero I, Rubino E, Valfre W, Gallone S, De Martino P, Zampella E *et al*. (2007). Association between the G1246A polymorphism of the hypocretin receptor 2 gene and cluster headache: a meta-analysis. *J Headache Pain* **8**: 152–156.

Sakamoto F, Yamada S, Ueta Y (2004). Centrally administered orexin-A activates corticotropin-releasing factor-containing neurons in the hypothalamic paraventricular nucleus and central amygdaloid nucleus of rats: possible involvement of central orexins on stress-activated central CRF neurons. *Regul Pept* **118**: 183–191.

Sakurai T, Amemiya A, Ishii M, Matsuzaki I, Chemelli RM, Tanaka H *et al*. (1998). Orexins and orexin receptors: a family of hypothalamic neuropeptides and G protein-coupled receptors that regulate feeding behavior. *Cell* **92**: 573–585.

Scammell TE, Saper CB (2005). Orexin, drugs and motivated behaviors. *Nat Neurosci* **8**: 1286–1288.

Sharf R, Sarhan M, Dileone RJ (2008). Orexin mediates the expression of precipitated morphine withdrawal and concurrent activation of the nucleus accumbens shell. *Biol Psychiatry* **64**: 175–183.

Siegel JM (2004). Hypocretin (orexin): role in normal behavior and neuropathology. *Annu Rev Psychol* **55**: 125–148.

Smart D, Sabido-David C, Brough SJ, Jewitt F, Johns A, Porter RA *et al*. (2001). SB-334867-A: the first selective orexin-1 receptor antagonist. *Br J Pharmacol* **132**: 1179–1182.

Taheri S, Sunter D, Dakin C, Moyes S, Seal L, Gardiner J *et al*. (2000). Diurnal variation in orexin A immunoreactivity and prepro-orexin mRNA in the rat central nervous system. *Neurosci Lett* **279**: 109–112.

Tang J, Chen J, Ramanjaneya M, Punn A, Conner AC, Randeva HS (2008). The signalling profile of recombinant human orexin-2 receptor. *Cell Signal* **20**: 1651–1661.

Thorpe AJ, Kotz CM (2005). Orexin A in the nucleus accumbens stimulates feeding and locomotor activity. *Brain Res* **1050**: 156–162.

Trivedi P, Yu H, MacNeil DJ, Van der Ploeg LH, Guan XM (1998). Distribution of orexin receptor mRNA in the rat brain. *FEBS Lett* **438**: 71–75.

Voisin T, Rouet-Benzineb P, Reuter N, Laburthe M (2003). Orexins and

their receptors: structural aspects and role in peripheral tissues. *Cell Mol Life Sci* **60**: 72–87.

Willie JT, Chemelli RM, Sinton CM, Tokita S, Williams SC, Kisanuki YY *et al*. (2003). Distinct narcolepsy syndromes in orexin receptor-2 and orexin null mice: molecular genetic dissection of non-REM and REM sleep regulatory processes. *Neuron* **38**: 715–730.

Winsky-Sommerer R, Boutrel B, de Lecea L (2005). Stress and arousal: the corticotrophin-releasing factor/hypocretin circuitry. *Mol Neurobiol* **32**: 285–294.

Winsky-Sommerer R, Yamanaka A, Diano S, Borok E, Roberts AJ, Sakurai T *et al*. (2004). Interaction between the corticotropin-releasing factor system and hypocretins (orexins): a novel circuit mediating stress response. *J Neurosci* **24**: 11439–11448.

Yamanaka A, Tsujino N, Funahashi H, Honda K, Guan JL, Wang QP *et al*. (2002). Orexins activate histaminergic neurons via the orexin 2 receptor. *Biochem Biophys Res Commun* **290**: 1237–1245.

Yoshida Y, Fujiki N, Nakajima T, Ripley B, Matsumura H, Yoneda H *et al*. (2001). Fluctuation of extracellular hypocretin-1 (orexin A) levels in the rat in relation to the light-dark cycle and sleep-wake activities. *Eur J Neurosci* **14**: 1075–1081.